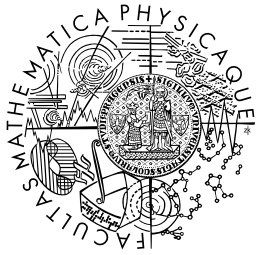

FACULTY
OF MATHEMATICS
AND PHYSICS
Charles University

BACHELOR THESIS

Martin Odehnal

The origin of Jupiter Trojans

Astronomical Institute of Charles University

Supervisor of the bachelor thesis: doc. Mgr. Miroslav Brož, Ph.D.
Study programme: Physics

Prague 2023

I declare that I carried out this bachelor thesis independently, and only with the cited sources, literature and other professional sources. It has not been used to obtain another or the same degree.

I understand that my work relates to the rights and obligations under the Act No. 121/2000 Sb., the Copyright Act, as amended, in particular the fact that the Charles University has the right to conclude a license agreement on the use of this work as a school work pursuant to Section 60 subsection 1 of the Copyright Act.

In ..... date ....

Author's signature

I would like to thank my supervisor, doc. Miroslav Brož, for all the advice, corrections, and his unrelenting enthusiasm for the subject, which was a great inspiration to me.

Title: The origin of Jupiter Trojans

Author: Martin Odehnal

Institute: Astronomical Institute of Charles University

Supervisor: doc. Mgr. Miroslav Brož, Ph.D.

Abstract: The Jupiter Trojans are a group of at least 12, 000 asteroids located in the vicinity of the Lagrange points L4 and L5. There are several theories for the origin of Trojans, such as the chaotic capture during the 1:2 resonance of Jupiter and Saturn, the Jumping Jupiter scenario, or the capture in a gaseous disk. New models, however, show important hydrodynamic phenomena in a gaseous disk during planetary migration, which could also affect Trojan capture, such as the growth of eccentricity or inclination of protoplanets (Chrenko et al. 2017, Eklund & Masset 2017).

We performed two-fluid hydrodynamic simulations of a protoplanetary disk consisting of gas and pebbles, with one 20 M_{E} Jupiter-like protoplanet rapidly growing via gas accretion, and computed trajectories and the capture efficiency of small asteroids, from 10 m up to 10 km in diameter. In our simulations, we found that 29 out of 100 hundred-meter planetesimals placed on circular orbits near the growing circular proto-Jupiter were captured in L4/L5. In the case of proto-Jupiter having non-zero initial eccentricity and inclination, the captured orbits of 100 m and 10 km planetesimals were unstable and eventually left the Trojan region. On the contrary, 10 m planetesimals stayed on stable orbits due to aerodynamic drag. The inclinations of captured planetesimals are very dependent on their initial inclinations. The eccentric and inclined proto-Jupiter did not excite their orbits above 3°, which is in stark contrast to the observed high inclinations of Trojans up to 30°. Therefore, our models require planetesimals to be already on high inclinations prior to capture, or an external dynamical excitation during the future evolution of the Solar System.

Keywords: Solar System, Asteroids, Jupiter, Trojans, Protoplanetary disk

Název práce: Původ Trojanů Jupitera

Autor: Martin Odehnal

Ústav: Astronomický ústav UK

Vedoucí bakalářské práce: doc. Mgr. Miroslav Brož, Ph.D.

Abstrakt: Trojané Jupiteru jsou skupinou více než 12 000 planetek nacházejících se v blízkosti Lagrangeových bodů L4 a L5. O původu Trojanů existuje vícero teorií, například zachycení při rezonanci 1:2 Jupiteru a Saturnu, teorie skákajícího Jupiteru nebo zachycení v plynném disku. Nové modely však ukazují důležité hydrodynamické jevy, které by mohly ovlivnit zachycování Trojanů, jako je růst excentricity a sklonu protoplanet (Chrenko et al. 2017, Eklund & Masset 2017).

Provedli jsme dvoutekutinové hydrodynamické simulace protoplanetárního disku složeného z plynu a z balvanů, s jednou protoplanetou o hmotnosti 20 M_{E}, odpovídající zárodku Jupiteru, která rychle roste díky akreci plynu. Spočetli jsme trajektorie a účinnosti zachycování planetesimál, s průměry od 10 m do 10 km. Ze 100 stometrových planetesimál umístěných na kruhových drahách poblíž rostoucího kruhového proto-Jupiteru se jich 29 zachytilo v okolí L4/L5. V případě, že proto-Jupiter měl nenulovou počáteční excentricitu a sklon, byly orbity zachycených 100m a 10km planetesimál nestabilní a časem opustily Trojanskou oblast. Naopak 10m planetesimály zůstaly na stabilních orbitách kvůli aerodynamickému tření. Sklony zachycených planetesimál jsou závislé na počátečních sklonech. Excentrický skloněný proto-Jupiter nedokázal sklony planetesimál vybudit nad 3°, což je v přímém rozporu s pozorovanými skony Trojanů až 30°. Naše modely tedy vyžadují, aby buď planetesimály měly vysoké sklony, nebo aby je následný vývoj Sluneční soustavy vybudil.

Klíčová slova: Sluneční soustava, planetky, Jupiter, Trojané, Protoplanetární disk

Contents

Trojans, what are they?

In December 1891, the German astronomer Max Wolf photographed an asteroid, which had the same orbital period as Jupiter, the asteroid is called (588) Achilles (Wolf 1892). A few years later another two similar asteroids were discovered by his colleague August Kopff, namely (617) Patroclus (Wolf 1906) and (624) Hektor (Wolf 1907). All these asteroids share orbital periods with Jupiter and are located about 60° ahead, or in the case of Patroclus 60° behind, Jupiter. We came to call these asteroids Jupiter Trojans (Nicholson 1961).

As of 2023, we have observed more than 12,000 Trojans. The population is split into two swarms orbiting two equilibrium points of the 3-body problem, known as L4 and L5. Observations show that the L4 swarm is substantially larger than the L5 swarm, with the populations being over 8,200 for the L4 and over 4,200 in the L5 swarm (*Minor Planet Center* 2023).

The Trojans orbit in the 1:1 mean-motion resonance with Jupiter, have eccentricities up to 0.15 and high inclinations up to 30°. The current distribution of eccentricities and inclinations of Trojans is shown in Figure 1. They orbit on tadpole orbits with the libration period of about 150 yrs and the full libration semi-amplitude is up to ±30°. The population mostly consists of D-types ($\sim$ 80%) and C/P-types ($\sim$ 20%) asteroids (Nesvorný 2018). There is a small number of collisional families among Trojans ($\sim$ 10), some are visible in Figure 1, the largest one is associated with the asteroid (3548) Eurybates (Brož & Rozehnal 2011, Rozehnal et al. 2016, Vinogradova 2020).

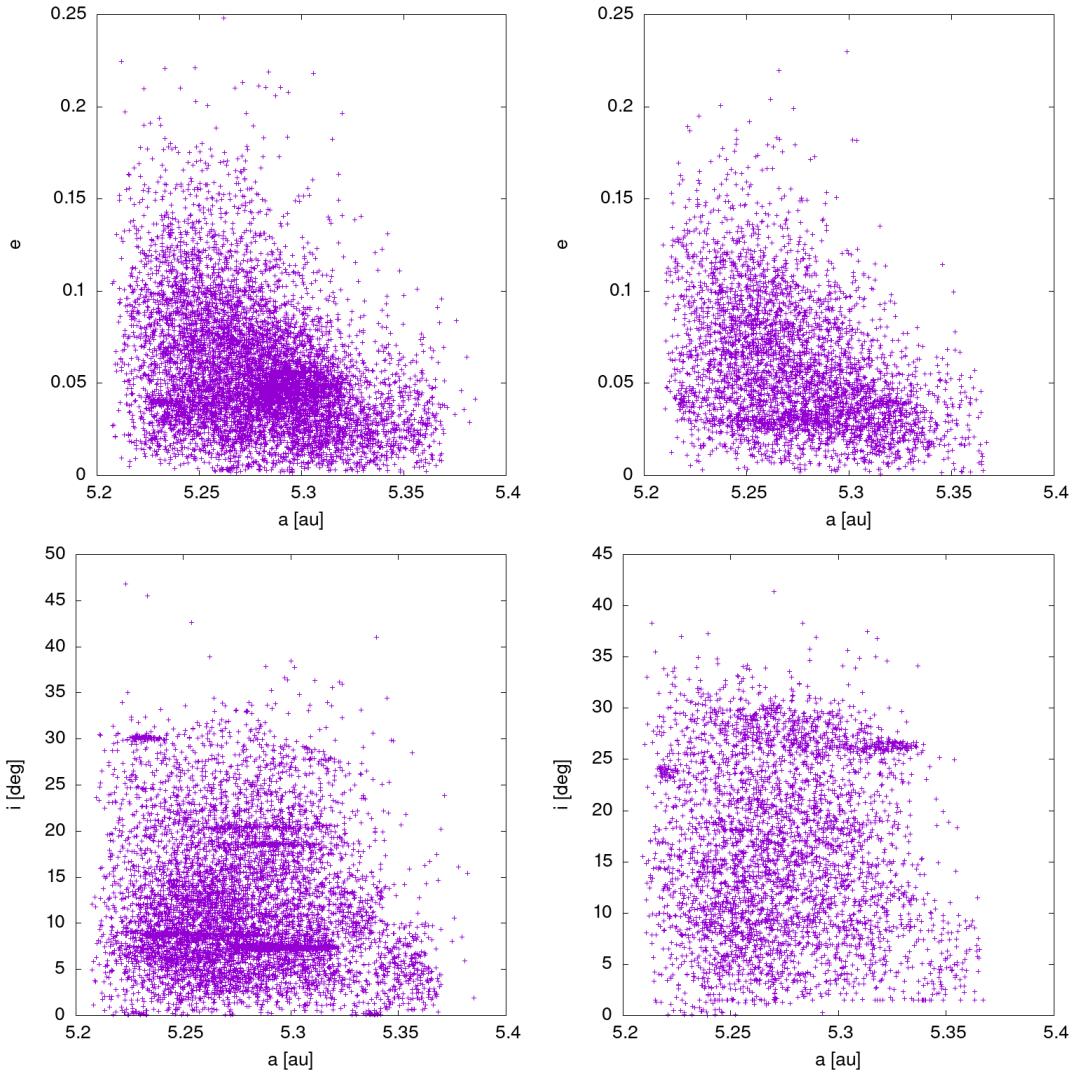

Figure 1: Observed distributions of Trojans, the proper semi-major axis versus the proper eccentricity (top) and the proper inclination (bottom), for the L4 (left) and L5 (right) swarms. There are visible asteroid families, esp. in the inclinations plot of the L4 swarm. The data were taken from Rozehnal et al. (2016).

1. Theories of Trojans origin

Jupiter Trojans are thought to have been captured from a much larger population of planetesimals that existed in the Solar System between 5 to 30 au during the formation of giant planets (Jupiter, Saturn, Uranus, Neptune).

First theories suggested that Trojans were captured during the early stages of Jupiter's growth, such as Marzari & Scholl (1998), who capture planetesimals using the changing gravity field of growing proto-planet. However, in those theories, Trojans ended up on very flat orbits with inclinations well under 10°. However this stands in sharp contrast to current observations, which show a wide distribution of inclinations up to 30°, shown in Figure 1.

In the following sections, we review new theories of Trojan capture that can explain the observed distribution of inclinations (Nesvorný 2018).

1.1 Capture during 2:1 resonance

The next theory is based on the Nice model (Tsiganis et al. 2005). In the model, the Solar System became unstable when Jupiter and Saturn crossed their mutual 2:1 mean-motion resonance. That is when Saturn's period was twice Jupiter's, $P_{\mathrm{Sat}}/P_{\mathrm{Jup}} = 2$. For comparison, the ratio today is 2.49, which is close to the 5:2 ratio, i.e. The great inequality (Lovett 1895). (Morbidelli et al. 2005) propose that Jupiter Trojans were trapped in orbits at the L_4 and L_5 points by chaotic capture during this particular 2:1 resonance.

This resonance creates chaos around Jupiter's L4 and L5 points, as the libration period in resonance 1:1 is close to 2:1. If a small body is scattered by somewhere near Jupiter's orbit, it can make its way to the vicinity of the L4 and L5 points. When the giant planets then leave the resonance, small bodies remain trapped by Jupiter. The random nature of the capture process results in asteroids being captured into all the possible stable orbits, which include small libration amplitudes and large inclinations.

A weakness of this model is, that the slow migration of Jupiter and Saturn past the 2:1 resonance, which is the defining feature of the Nice model, proves difficult to reconcile with the orbital structure of the asteroid belt (Morbidelli et al. 2010).

1.2 Jumping Jupiter scenario

The orbital structure of the asteroid belt, which can not be explained by the Nice model, could imply that the period ratio of Jupiter and Saturn must have had a discontinuity when they scattered one of the ice giants. This model is described in Morbidelli et al. (2010), and with a new model of the evolution of the Solar System, a new model of the Trojan capture must be constructed.

(Nesvorný et al. 2013) found that most of the Trojans were captured just after the closest encounter of Jupiter with the ice giant. The encounter drastically changed the semi-major axis of Jupiter by as much as 0.2 au in a single jump. The jump radially displaced Jupiter's already existing Trojans and led to capture

of new population of bodies, which happened to be where Jupiter was located after the jump.

The orbital distribution of stable Trojans obtained in their simulations closely matches the observed distributions, including orbits with small libration amplitudes, small eccentricities, and both small and large inclinations, which tend to be the most difficult to capture. Their model is also potentially capable of explaining the observed asymmetry of Jupiter Trojans (Szabó et al. 2007), which they attribute to late passages of the ice giant near L5, that presumably depleted the L5 population.

1.3 Capture in a gaseous disk

Up until now, the models we reviewed were based only on planetesimal disks. However, now we introduce models, which consider a gaseous disk. While in previous models only gravitational interactions were taken into account, these models also consider hydrodynamical effects like aerodynamic drag or pressure gradients in gas. As a result, they tend to focus on smaller objects (up to hundreds of meters), as hydrodynamical effects are more significant at this scale.

Lyra et al. (2009) focusses on centimeter- to meter-sized particles, which get within high-pressure regions, such as the L4 and L5 points of giant planets. There small particles have an opportunity to collapse and form larger planetesimals and even planetary embryos. In their models, the collapse occurs among particles smaller than 40 cm, and the formed proto-planets tend to have from $2\,M_E$ to $17\,M_E$, which is in the range of super-Earths to mini-Neptunes.

Although a Jupiter-sized planets could induce such formation of planetesimals and planetary embryos in the Trojan regions, they do not exist in the Solar System but could be common in exoplanets. The instabilities such as the Nice model or the migrating ice giant mentioned previously, could be the reason why this type of formation did not occurring in our Solar System.

A different model was proposed by Pirani et al. (2019), in which a rapid, large-scale planetary migration occurs in the Solar System. The migration manages to produce the observed asymmetry between the L4 and L5 populations. However, once again, the inclinations of captured Trojans are close to zero, thus the need for some other dynamical effects to excite the inclinations to observed high inclinations.

1.4 Growth of Jupiter's eccentricity and inclination

The main motivation for this work on Trojan's origin, is Chrenko et al. (2017), Eklund & Masset (2017) and Brož et al. (2021). They simulate planetary embryos growing by pebble accretion and study their migration and interactions. They find that orbital eccentricities of these embryos are considerably excited by the presence of the so-called "hot trail", an asymmetric overheated lobe of gas produced by accretion heating in the embryo's vicinity. Our study aims to investigate if this excitation of Jupiter's orbit by the aforementioned hot-trail effect affects also the Trojan capture.

2. Hydrodynamics of protoplanetary disks

In this thesis, we compute hydrodynamic simulations to study the evolution of protoplanetary disk, the migration of a planetary embryo, and their interaction with smaller planetesimals. The necessary physical laws and equations, that is the Eulerian hydrodynamics, are briefly reviewed in this Chapter.

We first describe the respective set of equations in 3-dimensional continuous vector form and then, in Section 2.2, we state the equations used in our simulations in 2-dimensional discretized component form and describe the Fargo-Thorin code itself (Chrenko et al. 2017).

2.1 3-dimensional, continuous, vector form

We use hte Eulerian formalism, where the flow of fluid, i.e., the temporal evolution of volumetric density ρ and velocity $\boldsymbol{v}$, is described with respect to a static observer. Let us first state the equations in a general form.

Continuity equation

The first equation, the continuity equation, generally describes a transport of some quantity. Its vector form is (Brož 2022)

$$\frac{\partial \rho}{\partial t} + \boldsymbol{v} \cdot \nabla \rho = -\rho \nabla \cdot \boldsymbol{v}, \tag{2.1}$$

where ρ denotes the volumetric density, and $\boldsymbol{v}$ the velocity. Every term in this equation can be expressed in units $\mathrm{kg\,m^{-3}\,s^{-1}}$. Such an equation is a local form of a conservation law. It says that mass can be neither created nor destroyed and it can not vanish from one place to appear at another, there must be a continuous flow between the two places.

Navier-Stokes equation

The second equation expresses the momentum conservation for fluids. The vector form of the equation is commonly called the Navier-Stokes (Brož 2022)

$$\begin{aligned}\frac{\partial \boldsymbol{v}}{\partial t} + \boldsymbol{v} \cdot \nabla \boldsymbol{v} = -\frac{1}{\rho}\nabla P - \nabla \Phi + \frac{1}{\rho \mu_{\mathrm{vac}}}(\nabla \times \mathbf{B}) \times \mathbf{B} \\ + \frac{1}{\rho}\left[\nabla \cdot \mu_1 \nabla \boldsymbol{v} + \nabla\left(\mu_2 + \frac{1}{3}\mu_1\right)\nabla \cdot \boldsymbol{v}\right],\end{aligned} \tag{2.2}$$

where the right-hand side describes the different accelerations acting on the fluid, therefore all of the terms are in units $\mathrm{m\,s^{-2}}$.

The most common acceleration on the right-hand side is the pressure gradient ∇P. This acceleration arises from the pressure force, which is present between two

places with different pressures. The second term is the gravitational acceleration, with Φ being the gravitational potential.

The third term, the Lorentz's term, corresponds to the well-known formula $\boldsymbol{F} = q(\boldsymbol{E} + \boldsymbol{v} \times \mathbf{B})$, where the macroscopic electric field $\boldsymbol{E}$ in plasma is zero, the current density $\boldsymbol{j} = \rho_Q \boldsymbol{v}$ can be expressed form the Ampere's law $\mu_{\text{vac}}\boldsymbol{j} = \nabla \times \mathbf{B}$. Here, q denotes the electric charge, ρ_Q the charge density, μ_{vac} the vacuum permeability, $\mathbf{B}$ the magnetic induction.

The last two terms are called the viscous terms, namely the friction between two neighbouring layers of the fluid, flowing at different velocities. The force acting on a unit surface is called stress (unit Pa) The friction for Newtonian fluids is proportional to the gradient of velocity, $\mu_1 \nabla \boldsymbol{v}$, where μ_1 denotes the dynamical viscosity. An acceleration arises only if the stress values from the top layer and the bottom layer change. The last one describes the volumetric viscosity, with μ_2 as the dynamical volumetric viscosity.

Energy equation

The third equation is similar to the first one, but instead of the mass density $\sim \rho$, we use the energy density U. The energy equation in the vector form is (Brož 2022)

$$\frac{\partial U}{\partial t} + \boldsymbol{v} \cdot \nabla U = -U \nabla \cdot \boldsymbol{v} - P \nabla \cdot \boldsymbol{v} - \kappa_{\text{P}} \rho c a T^4 + \kappa_{\text{P}} \rho c E_{\text{rad}} - \nabla \cdot F_\star \hat{r} + \nabla \cdot K \nabla T. \quad (2.3)$$

The equation can be derived from the 1st law of thermodynamics, and all terms are in units $\mathrm{J\,m^{-3}\,s^{-1}}$. The first term on the right-hand side describes the internal energy taken from gas by expansion ($-U \nabla \cdot \boldsymbol{v}$). The second term is the energy used for mechanical work ($-P \nabla \cdot \boldsymbol{v}$).

All the remaining terms are the heat sources. Two terms are describing radiation emission and absorption, $-\kappa_{\text{P}} \rho c a T^4 + \kappa_{\text{P}} \rho c E_{\text{rad}}$, where κ_{P} stands for the Planck mean absorption coefficient, ρ the volumetric density, a the radiative constant, c the speed of light, and T the thermodynamic temperature. The next term is the irradiance, $-\nabla \cdot F_\star \hat{r}$, $F_\star$ stands for the radiant flux received from the Sun and $\hat{r}$ the unit position vector. The last term describes the thermal diffusion, $\nabla \cdot K \nabla T$, where T denotes again the thermodynamical temperature and K the thermal conductivity.

Ideal gas law

The last necessary equation is the ideal gas law, or the equation of state. Its form is

$$P = \frac{\rho}{\mu m_{\text{u}}} k T, \quad (2.4)$$

with k standing for the Boltzmann constant, μ the mean molecular weight and m_{u} the atomic weight.

This equation is a good approximation of the behavior of gas, however, since it only accounts for the volume $V = m/\rho$, the temperature T, and the pressure P, it neglects molecular size and intermolecular attractions, which become less important for lower densities such as the gas in our disk.

2.2 Implementation in the Fargo-Thorin code

In this study, we use the 2-dimensional hydrodynamic code Fargo-Thorin by Chrenko et al. (2017), which itself is a heavily modified version of the FARGO (Masset 2000). The code is an Eulerian solver on a polar staggered mesh, modified to account for interactions between planetary embryos, a gas disk, and also a pebble disk. In this section, we describe how the hydrodynamic equations from Section 2.1 are actually implemented in the code.

The first thing we need to mention is that the code is 2D, thus solving 2D equations and using the surface density Σ. Nevertheless the description accounts for vertical stratification to approximate effects that are dependent on the 3D disk. This is done by using the Gaussian profile, therefore, the volumetric density ρ is

$$\rho(r,\theta,z) = \frac{\Sigma(r,\theta)}{\sqrt{2\pi}H(r,\theta)}\exp\left(-\frac{z^2}{2H^2(r,\theta)}\right), \tag{2.5}$$

where $H = c_\mathrm{s}/(\sqrt{\gamma}\Omega_\mathrm{K}$ denotes the local pressure scale height, $c_\mathrm{s} = \sqrt{\gamma P/\Sigma}$ the isothermal sound speed, $\gamma = 1.4$ the adiabatic index, Ω_K the Keplerian angular frequency, and z the vertical coordinate.

2.2.1 Continuity equation

As the Fargo-Thorin code is 2-dimensional, the equations from Section 2.1 have to be integrated in the vertical dimension. The new continuity equation is

$$\frac{\partial\Sigma}{\partial t} + \nabla\cdot(\Sigma\boldsymbol{v}) = 0, \tag{2.6}$$

where Σ is the gas surface density and $\boldsymbol{v}$ is the vertically averaged gas flow velocity.

2.2.2 Navier-Stokes equation

The 2D vector form of the Navier-Stokes equation is

$$\frac{\partial\boldsymbol{v}}{\partial t} + \boldsymbol{v}\cdot\nabla\boldsymbol{v} = -\frac{1}{\Sigma}\nabla P + \frac{1}{\Sigma}\nabla\cdot T_\nu - \frac{\int\rho\nabla\Phi dz}{\Sigma} + \frac{\Sigma_p}{\Sigma}\frac{\Omega_\mathrm{K}}{\tau}(\boldsymbol{V}-\boldsymbol{v}), \tag{2.7}$$

where P is the vertically integrated pressure, T_ν the viscous stress tensor, ρ the volumetric density, Φ the gravitational potential. The last term describes the interaction between the gas and pebble disks, Σ and Σ_p denote surface densities, $\boldsymbol{v}$ and $\boldsymbol{V}$ their velocities, τ the Stokes number.

Now we will state the equations in a discretized form as implemented in the code. They are written in the polar coordinates with i representing the radial component and j the azimuthal component. Notice, we have to average the scalar quantities from two neighboring cells. This is because, in the staggered mesh, the scalar quantities are cell-centered as opposed to vector quantities, which are face-centered. Namely, one time step is Δt and the explicit solution is

$$(v_{\rm rad})_{i,j} = (v_{\rm rad})_{i,j} + \Delta t\Big\{-\nabla(P_{\rm rad})_{i,j} + 0.5(\Phi_{i,j} + \Phi_{i-1,j}) + \\ + \left[\frac{1}{4}\Big((v_\theta)_{i,j} + (v_\theta)i, j-1 + (v_\theta)_{i-1,j} + (v_\theta)_{i-1,j-1}\Big) + R_i\Omega_{\rm K}\right]^2 \frac{1}{R_i} - \\ - \frac{2((q_{\rm rad})_{i,j} - (q_{\rm rad})_{i-1,j}}{\rho_{i,j} + \rho_{i-1,j}} \frac{1}{(R_{\rm med})_i - (R_{\rm med})_{i-1}}\Big\}, \quad (2.8)$$

$$(v_\theta)_{i,j} = (v_\theta)_{i,j} + \Delta t((-\nabla(P_{\rm rad})_{i,j}) + 0.5[\Phi_{i,j} + \Phi_{i,j-1}] - \\ - \left[\frac{2[(q_\theta)_{i,j} - (q_\theta)_{i,j-1}]}{\rho_{i,j} + \rho_{i,j-1}} \frac{2\pi R_{\rm med}}{n}\right], \quad (2.9)$$

$$\nabla(P_{\rm rad})_{i,j} = \frac{2(P_{i,j} - P_{i-1,j})}{\rho_{i,j} + \rho_{i-1,j}} \frac{1}{(R_{\rm med})_i - (R_{\rm med})_i}, \quad (2.10)$$

$$\nabla(P_\theta)_{i,j} = \frac{2(P_{i,j} - P_{i,j-1})}{\rho_{i,j} + \rho_{i,j-1}} \frac{2\pi R_{\rm med}}{ns}, \quad (2.11)$$

$$(R_{\rm med})_i = \frac{2}{3}\frac{R_{i+1}^3 - R_i^3}{R_{i+1}^2 - R_i^2}, \quad (2.12)$$

$$(q_{\rm rad})_{i,j} = (1.41)^2\rho_{i,j}((v_{\rm rad})_{i+1,j} - (v_{\rm rad})_{i,j})^2, \quad (2.13)$$

$$(q_\theta)_{i,j} = (1.41)^2\rho_{i,j}((v_\theta)_{i,j+1} - (v_\theta)_{i,j})^2, \quad (2.14)$$

where $v_{\rm rad}$ denotes the perturbation of velocity in radial direction after the time step, v_θ the azimuthal velocity after the time step, n the number of azimuthal cells in the mesh, R the radius from the center of the Solar System.

2.2.3 Energy sources terms

The energy equation implemented in Fargo-Thorin is

$$\frac{\partial U}{\partial t} + \nabla \cdot (U\boldsymbol{v}) = -P\nabla \cdot \boldsymbol{v} + Q_{\rm visc} + Q_{\rm irr} + Q_{\rm acc} - Q_{\rm rad}. \quad (2.15)$$

In order to avoid unnecessary time restriction, Chrenko et al. (2017) solve this equation implicitly.

Let us state the energy source terms in detail (Chrenko et al. 2017).

The term $Q_{\rm visc}$ stands for the viscous dissipation heating and is calculated as

$$Q_{\rm visc} = \frac{1}{2\nu\Sigma}(\tau_{rr}^2 + 2\tau_{r\theta}^2 + \tau_{\theta\theta}^2) + \frac{2\nu\Sigma}{9}(\nabla \cdot \boldsymbol{v})^2, \quad (2.16)$$

where ν is the kinematic viscosity and τ_{ij} components of the viscous stress tensor T_ν.

The stellar irradiation represented by the term $Q_{\rm irr}$ describes the energy gained from solar radiation

$$Q_{\rm irr} = \frac{2\sigma_R T_{\rm irr}^4}{\tau_{\rm eff}}, \quad (2.17)$$

where σ_R is the Stefan-Boltzmann constant, τ_{eff} the effective optical depth. The irradiation temperature T_{irr} is obtained as the projection of the stellar radiation flux onto the disk surface,

$$T_{\text{irr}}^4 = (1 - A) \left(\frac{R_\star}{r} \right)^2 T_\star^4 \sin \alpha, \tag{2.18}$$

where A stands for the disk albedo, $T_\star$ the effective temperature of the protostar, $R_\star$, its radius, and α the angle at which the starlight strikes the disk.

The planetary embryos that accrete gas also radiate heat, depending on their accretion rate. The embryo heats the grid cell it is embedded in and the power of such heating is

$$Q_{\text{acc}} = \frac{1}{S} \frac{GM_{\text{emb}}}{R_{\text{emb}}} \frac{\mathrm{d}M_{\text{emb}}}{\mathrm{d}t}, \tag{2.19}$$

where S stands for the cell area, G the gravitational constant, and M_{emb} and R_{emb}, respectively, are the mass and radius of the embryo.

The last term describes the energy from radiative transfer.

$$Q_{\text{rad}} = \frac{2\sigma_R T^4}{\tau_{\text{eff}}} + 2H \nabla \cdot \boldsymbol{F}. \tag{2.20}$$

This first term is complementary to Q_{irr} and it is assumed that most of the energy is transported by radiation in the vertical direction, T is the temperature in the midplane. The last term describes radiative diffusion as the divergence of radiant flux.

2.2.4 Pebble disk

The pebbles are treated as a fluid, described solely by hydrodynamical quantities, the surface density Σ_{p} and the velocities V_{r}, V_θ, together with several parameters, like the Stokes number τ. It describes aerodynamic properties of pebbles which are partly coupled to gas Chrenko et al. (2017),

$$\tau = \frac{\rho_{\text{b}} R_{\text{p}}}{\rho_0 c_{\text{s}}} \Omega_{\text{K}}, \tag{2.21}$$

where ρ_{b} stands for the pebble bulk density, R_{p} the pebble size, ρ_0 the midplane volume density, c_s the sound speed and Ω_{K} the Keplarian angular frequency.

Pebble flow and accretion onto protoplanets is described by the equation

$$\frac{\partial \Sigma_{\text{p}}}{\partial t} + \nabla \cdot (\Sigma_{\text{p}} \boldsymbol{V}) = \left(\frac{\partial \Sigma_{\text{p}}}{\partial t} \right)_{\text{acc}}. \tag{2.22}$$

The accretion acts as a mass sink and the removed mass is accreted by the growing embryos.

After the accretion is resolved, the Stokes number gets recalculated, then the velocity fields are updated using the pebble fluid motion equation

$$\frac{\partial \boldsymbol{V}}{\partial t} + \boldsymbol{V} \cdot \nabla \boldsymbol{V} = \frac{\int \rho_{\text{p}} \nabla \Phi \mathrm{d}z}{\Sigma_{\text{p}}} - \frac{\Omega_{\text{K}}}{\tau} (\boldsymbol{V} - \boldsymbol{v}), \tag{2.23}$$

where ρ_{p} is the volumetric density of pebbles, Φ the gravitational potential and $\boldsymbol{v}$ the velocity of gas. Finally, all the quantities are advected using the Fargo transport algorithm (Masset 2000) as for the gas.

3. Models of planetesimal capture by growing Jupiter

In order to study how Jupiter captures Trojans in a gaseous disk and how the capture efficiency changes with different eccentricities and inclinations, we perform multiple simulations using the dynamical model from Chapter 2. We start with zero eccentricities and inclinations of Jupiter and 100 m planetesimals and little by little changes of the initial conditions.

3.1 Initial and boundary conditions

We simulate a protoplanetary disk with one planetary core, the $20\,\mathrm{M_E}$ (Earth mass) proto-Jupiter, which has already migrated close to its current position and is about to enter the runaway accretion stage (Pollack et al. 1996). The initial setup of the disk is mostly taken from Brož et al. (2021). The important disk parameters chosen for this simulation are summarized in Table 4.1.

The initial relaxed hydrodynamic profile of the disk is assumed to be symmetric in azimuth.

The disk is radially constrained by the inner boundary at $r_{\mathrm{min}} = 2.8\,\mathrm{au}$ and the outer boundary at $r_{\mathrm{max}} = 16\,\mathrm{au}$. In addition, there are set wave-killing zones (Chrenko et al. 2017). The zones are adjacent to the boundaries and cover intervals $[r_{\mathrm{min}}, 1.2r_{\mathrm{min}}]$ and $[0.9r_{\mathrm{max}}, r_{\mathrm{max}}]$. In these zones, a hydrodynamic quality (the surface density Σ, the energy U, the azimuthal velocity v_θ) is being damped towards the reference values obtained after the initial relaxation, or for the case of radial velocity v_r, to zero. Each time the boundary condition is applied, the following equation is solved in the zones (Chrenko et al. 2017)

$$\frac{\mathrm{d}q}{\mathrm{d}t} = -\frac{q - q_0}{t_{\mathrm{damp}}} f(r), \tag{3.1}$$

where q and q_0 represent said hydrodynamic quality. The time scale is set as $t_{\mathrm{damp}} = 0.1T_{\mathrm{orb}}$, which means one-tenth of the Keperian orbital period on the boundary. The $f(r)$ denotes a dimensionless ramp function that decreases from 1 at the boundary to 0 at the start of the wave-killing zone.

The computational polar mesh is divided into 512 radial rings and 768 azimuthal sectors. The maximum time step is $\Delta t = 3.725\,[\mathrm{c.u._t}] = 0.16\,\mathrm{yr} = 1/20\,P_{\mathrm{orb}}$ at 5.2 au, with output every 1000 steps, which is 2,200 yrs. The code units for time are $\mathrm{c.u._t} = \frac{1}{2\pi}\mathrm{sidereal\,yr} = \sqrt{\frac{1\,\mathrm{AU}}{\mathrm{GM_\odot}}}$. The time step is controlled by the CFL condition, which is calculated at every step using

$$\mathrm{d}t = \frac{0.5}{\sqrt{(\frac{c_\mathrm{s}}{\mathrm{d}x})^2 + \frac{v_\mathrm{rad}}{\mathrm{d}x_\mathrm{rad}} + \frac{v_\theta}{\mathrm{d}x_\theta} + 4c_\mathrm{vNR}^2 \frac{\mathrm{d}v}{\mathrm{d}x} + \frac{4\nu}{dx^2}}}, \tag{3.2}$$

where v_rad and v_θ are the radial and the azimuthal velocities, $\mathrm{d}x_\mathrm{rad}$ and $\mathrm{d}x_\theta$ are the sizes of current cell. When using the unindexed variables v and $\mathrm{d}x$, it was assumed that the lower of the radial and azimuthal values was used. c_s stands

for the speed of sound, ν for kinematic viscosity and c_{vNR}, the von Neumann-Richtmyer viscosity constant, valued at 1.41.

All of our simulation were calculated on the faculty Chimera cluster via the SLURM scheduling system. Each simulation used 50 CPUs and ran for around one day. We had to limit the number of particles to 100, because some particles got captured as Jupiter's moons, which resulted in severe time step limitations of the N-body integrator.

Viscosity. We use a fixed value of the kinematic viscosity $\nu = 5.0 \times 10^{14}\,\mathrm{cm^2\,s^{-1}}$. The relation between the kinematic and the dynamical viscosity μ is

$$\nu = \frac{\mu}{\rho}, \tag{3.3}$$

where ρ is the volumetric density of the fluid. The kinematic viscosity ν is often parametrized as (Shakura & Sunyaev 1973)

$$\nu = \alpha c_{\mathrm{s}} H, \tag{3.4}$$

where α is a free parameter, c_{s} the speed of sound, and H the vertical scale height. If we use our fixed ν to compute α, the corresponding value is $\alpha \approx 0.005$. This is relatively large value, suitable for an active, turbulent disk, with a magneto-rotational instability (MRI; (Balbus & Hawley 1991))

Gas surface density. The initial surface density at 1 au chosen for our simulation was $\Sigma_0 = 200\,\mathrm{g\,cm^{-2}}$. This value is lower then the Minimal Mass Solar Nebula (MMSN) (Hayashi 1981), so there is just enough gas around proto-Jupiter for it to grow to its current mass of $317\,\mathrm{M_E}$.

The gas surface density initially follows a power law $\Sigma = \Sigma_0 r^{-0.5}$. Using this exponent, we can estimate the initial surface density at 5.2 au, i.e., $87\,\mathrm{g\,cm^{-2}}$, which is slightly higher, but comparable to the surface densities used in Pollack et al. (1996), who use $\Sigma_0 = 750\,\mathrm{g\,cm^{-2}}$ but the power law exponent -1.5.

Figure 3.1 shows the surface density profile of the disk, after 9 kyr of evolution. The proto-Jupiter is already around $300\,\mathrm{M_E}$ and has opened a gap.

3.2 Models for 100 m asteroids

Our first simulation was set up with proto-Jupiter placed at 5.2 au, having size $20\,\mathrm{M_E}$ and just entering runaway accretion, thus opening a gap. Initially, the proto-Jupiter has no eccentricity and a very low inclination of 0.057°. We populated a hundred 100 m planetesimals on orbits right behind the proto-Jupiter's Hill sphere, from 5.34 au to 5.51 au. These planetesimals had zero eccentricities and the inclinations were in the interval $[0, 0.01°]$.

The simulation was run for 11 kyr, which is about 920 Jupiter orbits. In the course of time, we observed a rapid increase of proto-Jupiter's mass by accretion, similarly as in Pollack et al. (1996). Our proto-Jupiter grows from its starting mass $20\,\mathrm{M_E}$ to almost $300\,\mathrm{M_E}$. With the fast accretion, the proto-Jupiter immediately began to open a gap and slowly migrated inwards due to the Type-II migration. During our simulation, it moves from 5.20 au to 4.94 au.

Table 3.1: Summary of parameters for our hydrodynamical model of protoplanetary disk

Parameter	Notation	Value
Kinematic viscosity	ν	$5.0 \times 10^{14}\,\mathrm{cm^2\,s^{-1}}$
Gas surface density	Σ_0	$200\,\mathrm{g\,cm^{-2}}$
Rosseland mean opacity	κ	Zhu et al. (2012)
Vertical opacity drop	c_κ	0.6
Disk albedo	A	0.5
Stellar radius	R_S	$1.5\,\mathrm{R_S}$
Effective stellar temperature	T_S	4370 K
Initial aspect ratio	h	0.05
Pebble bulk density	ρ_p	$1\,\mathrm{g\,cm^{-3}}$
Pebble radial mass flux	M_F	$2 \times 10^{-4}\,\mathrm{M_E\,yr^{-1}}$
Inner radial boundary	r_min	2.8 au
Outer radial boundary	r_max	16 au
Radial mesh resolution	N_r	512
Azimuthal mesh resolution	N_θ	768

3.2.1 Aerodynamical acceleration

A planetesimal on a circular orbit at 5.35 au has the total acceleration of $a = 2.08 \times 10^{-4}\,\mathrm{m\,s^{-2}}$. This value is almost entirely due to the gravitational acceleration. For eccentric orbits, the acceleration changes periodically, depending on the position of the planetesimal along the orbit. For $e = 0.05$, the pericenter is 4.94 au from the Sun and the apocenter is 5.46 au, so the corresponding gravitational accelerations are $1.9 \times 10^{-4}\mathrm{m\,s^{-2}}$ and $2.3 \times 10^{-4}\mathrm{m\,s^{-2}}$.

We would like to compare these values to accelerations arising from aerodynamic drag. This can be calculated from Stokes' formula

$$a = \frac{1}{2} C \frac{S}{m} \rho v_\mathrm{rel}^2, \tag{3.5}$$

where C is a constant $C = 0.48$, v_rel the relative speed of planetesimal with respect to gas, and ρ the volumetric density of gas in the disk.

In our simulation, we use the surface density Σ described in more detail in Section 3.1. From surface density we can calculate the volumetric density using

$$\rho = \frac{\Sigma}{\sqrt{2\pi} H}, \tag{3.6}$$

where H is the height of the disk:

$$H = \frac{c_\mathrm{s}}{\sqrt{1.4}\Omega_\mathrm{k}} \tag{3.7}$$

For reference, we can calculate ρ at $a = 5.2$ au as $1 \times 10^{-10}\,\mathrm{kg\,m^{-3}}$

Now we can calculate the effect of drag. If we have a 100 m planetesimal on a circular orbit at 5.35 au, the aerodynamic acceleration a_drag is stable, around $1 \times 10^{-10}\,\mathrm{m\,s^{-2}}$. For the eccentric or inclined orbit ($e = 0.05, i = 5°$), acceleration peaks around $1 \times 10^{-7}\,\mathrm{m\,s^{-2}}$.

For comparison, drag needs at least 24 days, or 0.005 Jupiter orbits, to have an effect similar to gravity.

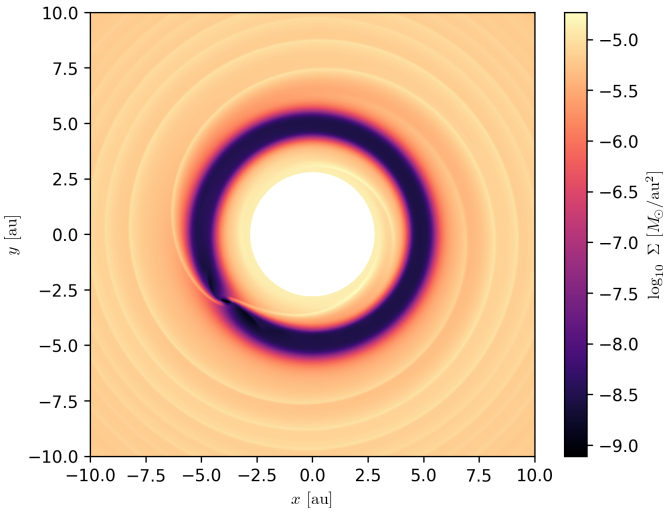

Figure 3.1: Surface density profile of the disk with one massive protoplanet, after 9 kyr of evolution. The proto-Jupiter is 300 M_E has created spiral arms and has opened a gap.

3.2.2 Detection of capture

The main reason for our simulations is to look at planetesimal capture after the interaction with Jupiter. The simulation is conveniently set up, so every planetesimal interacts with Jupiter within the first few hundred years. This is done by initially placing our planetesimals near the Hill sphere of rapidly expanding proto-Jupiter, which almost doubles in size during 300 years. Therefore, its Hill sphere increases and planetesimals orbiting near it find themselves in a perfect position to be captured as Trojans. Of the 100 planetesimals, 29 were captured this way. All bodies start on very cold orbits (have initial eccentricities and inclinations close to zero), therefore, the capture efficiency increases the closer the planetesimal starts to proto-Jupiter. If a planetesimal starts below 5.4 au, the efficiency of its capture is almost 75%.

All captures in our model occured during the planetesimals' first corotation orbits. When the proto-Jupiter catches up to the planetesimal for the first time, if it is close enough, it either captures it and sends it on a horseshoe orbit, or if the planetesimal is further away, it is sent on an eccentric orbit outwards or inwards. This first interaction happens during the first 320 years of simulation, or 27 Jupiter orbits.

We detect these captures by looking at the semimajor axis, if the semimajor axis of a planetesimal stays inside proto-Jupiter's Hill sphere radius, we detect the planetesimal as captured. This process can be seen in Figure 3.2.

3.2.3 Analysis of captured asteroid trajectories in L4 and L5

The captured planetesimals start orbiting as Trojans on horseshoe orbits, they librate around 180° from proto-Jupiter and their orbits encompass both Lagrangian points L4 and L5. In later phases, planetesimals begin to transition from full horseshoe orbits to very extended tadpole orbits (orbits around the L4 or L5 points), with large amplitudes of libration, reaching almost 180°. The libration amplitudes of planetesimals caught in the L4 cloud tend to be by about $5 - 10°$

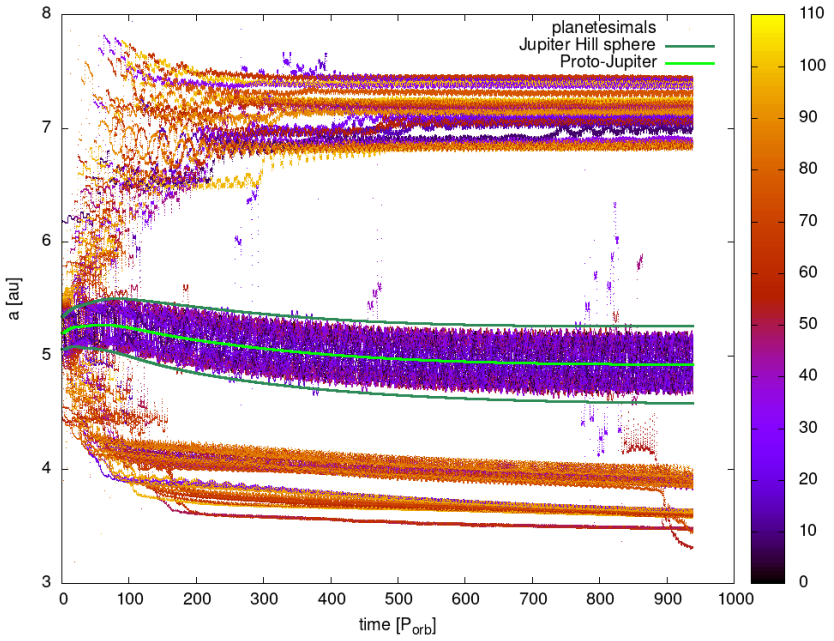

Figure 3.2: Temporal evolution of the semi-major axes for one hundred 100 m planetesimals and proto-Jupiter. The planetesimals are indicated in the color palette and arranged by their initial semi-major axis, with the number one corresponding to 5.34 au and number 100 to 5.51 au. Proto-Jupiter was migrating and rapidly accreting gas, reaching up to 300 M_{E}. Both Jupiter and its Hill sphere are indicated in green. The proto-Jupiter causes perturbations to free planetesimals orbiting around 4 au and 7 au. This is discussed in greater detail in Section 3.2.4. A total of 29 planetesimals were captured as Trojans when their semi-major axes were within the Hill sphere of the proto-Jupiter.

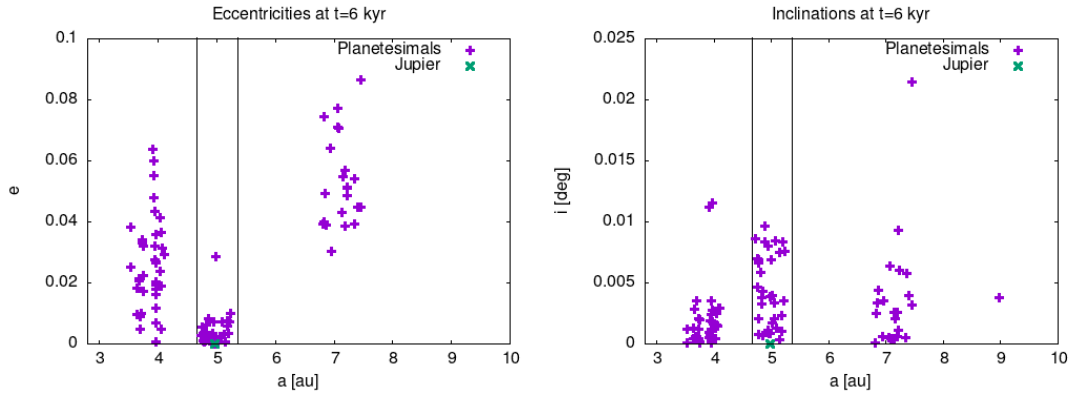

Figure 3.3: Eccentricity e (left) and inclination i (right) versus semimajor axis a of proto-Jupiter and 100 planetesimals from the first simulation after 6 kyr of evolution. Proto-Jupiter has an initial mass 20 $\mathrm{M_E}$, and planetesimal are 100 m in diameter, set right outside of proto-Jupiter's Hill sphere. Both proto-Jupiter and the planetesimals have zero initial eccentricities and inclinations. Proto-Jupiter's Hill sphere is highlighted by vertical lines. Some planetesimals were captured as Trojans, located inside the proto-Jupiter's Hill sphere. Their eccentricities are low (under 0.01) compared to other planetesimal scattered by proto-Jupiter, which are subsequently damped down by drag. The inclinations stay very low for both captured and scattered planetesimals, under 0.01°. We can compare this figure to similar Figures (3.9, 3.10, 3.11), where we modify the initial eccentricities and inclinations.

shorter than their L5 counterparts and also 10° further from proto-Jupiter.

As shown in Figure 3.4, the drag decreases the libration amplitude at a rate of 10° every 3-5 kyr. During our 11 kyr simulation, the tadpole orbits shorten by up to 40°. By extrapolation, we can assume, it would take at least 40 kyr for the planetesimals to reach zero amplitudes in L4/L5.

The trajectories of planetesimals closely resemeble the streamlines of gas in Figure 3.5. The similarity is due to the three-body problem. There are notable differences between streamlines near L4 and L5, which also correspond to the different libration amplitudes mentioned above.

Figure 3.6 shows the libration periods of captured planetesimal at the end of our simulation. We can see that the libration period on a tadpole orbit is at that time between 15 to 20 Jupiter orbits or 180-240 yr. There is no significant difference between the L4 and L5 populations, with 10 planetesimals orbiting around the L4 point and 10 planetesimals around L5. The remaining 9 planetesimals stayed on horseshoe orbits. However, our sample size is very small.

The planetesimals in this first simulation have zero eccentricities and very small inclinations, these values do not change significantly for the captured planetesimals, i.e. Figure 3.3. With the eccentricities and inclinations being so low, the tadpole orbits are very cold. This is all in stark contrast to observations, because the observed inclinations of Trojans are as high as 30°, i.e. Figure 1. Achieving high inclinations of captured planetesimals will be the focus of our second simulation.

The total mass of Trojans. Current estimates of the total mass of Trojans are as per Vinogradova & Chernetenko (2015) $(0.30 \pm 0.19) \times 10^{-10}\, M_{\mathrm{S}}$. This number is an extrapolation from physical characteristics and includes small asteroids. If we assume all Trojans came from this kind of capture, for which we have calculated the capture efficiency as 29%, the minimal planetesimal population in the feeding zone must have been $3 \times 10^{-5}\, M_{\mathrm{E}}$. In our simulation, the feeding zone is from 5.342 au to 5.514 au. With the metalicity of 0.01, the total mass of solids in the feeding zone would be $0.18\, M_{\mathrm{E}}$, of which $0.03\, M_{\mathrm{E}}$ are pebbles. The minimal population of Trojans needs to be only 0.006% of the total mass, which is not surprising as planetesimals contain only a tiny fraction of total solid mass. Most of the solid mass would already already part of the proto-Jupiter's core.

3.2.4 Analysis of free asteroid trajectories

Planetesimals that encountered proto-Jupiter and did not get captured as its Trojans, were diverted on highly eccentric orbits and flung either inwards or outwards. These orbits are then damped by drag, from eccentricities up to 0.3 right after the close encounter to up to 0.05 after 10 kyr of evolution, see Figure 3.3.

We are not examining the planetesimals flung outwards, because our model only contains proto-Jupiter and not other giants, which could interact with these planetesimals on their way to the become the Centaurs.

The planetesimals diverted inwards were flung to around 4 au, and from there, they began a slow migration inwards driven by drag, not getting captured by Jupiter's resonances. The temporal evolution of their semi-major axes is plotted in Figure 3.7. Even though no planetesimal got captured in the resonances, their

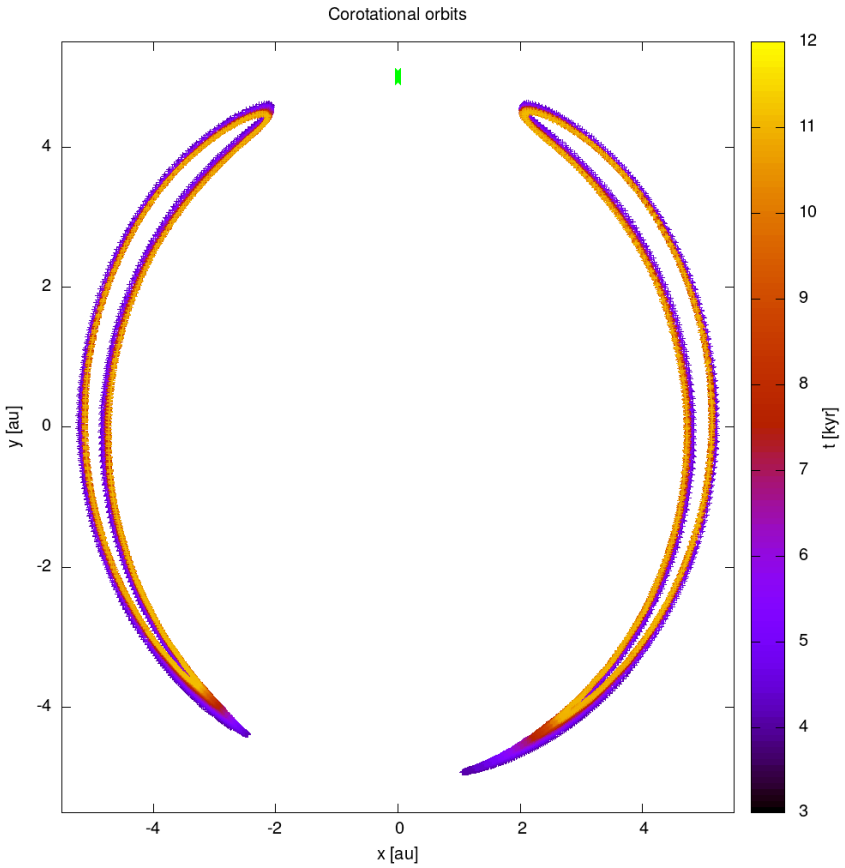

Figure 3.4: Examples of planetesimals captured on tadpole orbits, shown in the X, Y plane. The time span is from 4 to 11 kyr. The coordinate system is corotating with Jupiter (green cross). There is an apparent decrease in the libration amplitude of tadpole orbits for both bodies, due to drag. There is also a notable difference in the libration amplitude for the two bodies, with the L5 orbit (right) being about 10° longer and 5° closer to proto-Jupiter.

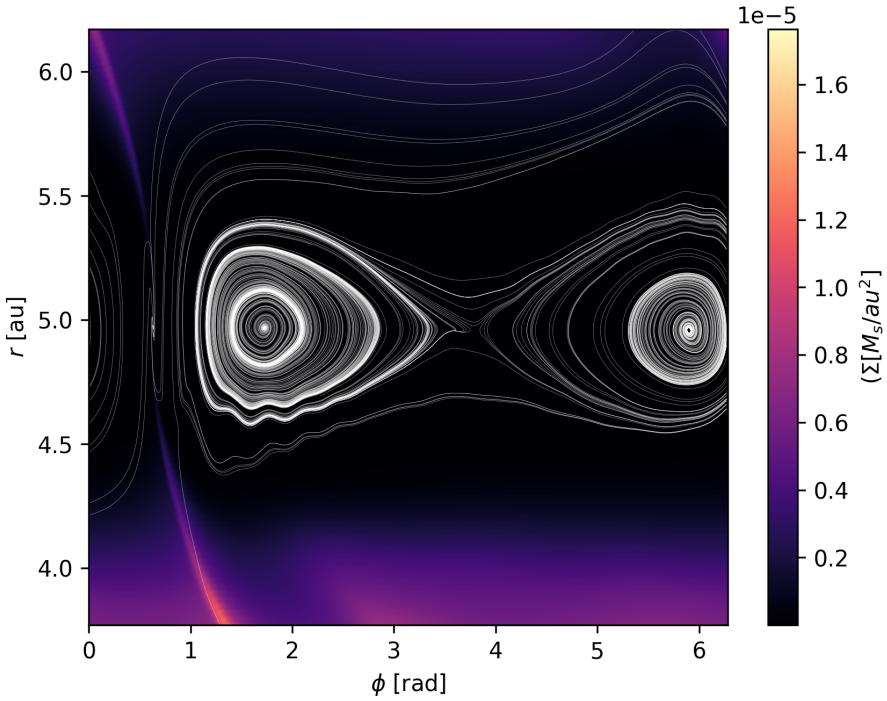

Figure 3.5: Gas streamlines inside proto-Jupiter's gap in the disk after 9 kyr. The background color shows the surface density Σ in the disk. The lagrange points L4 and L5 are clearly visible. The L4 orbits are slightly larger than the L5. Planetesimals in our simulations orbit similarly to the outer lines and slowly make their way inwards.

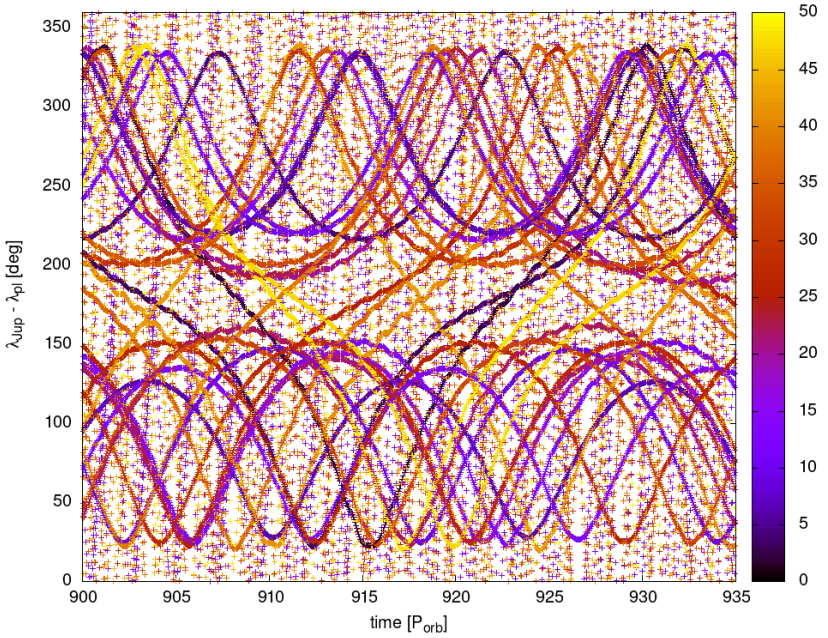

Figure 3.6: The libration amplitude and phase $\lambda_{\mathrm{Jup}} - \lambda_{\mathrm{pl}}$ of captured planetesimals in degrees during the last 420 yrs of the first simulation. The libration periods on tadpole orbits are around 200 yr. The number of planetesimals in both the L4 and L5 swarms is 10, remaining 9 are on horseshoe orbits, with periods of around 420 yr.

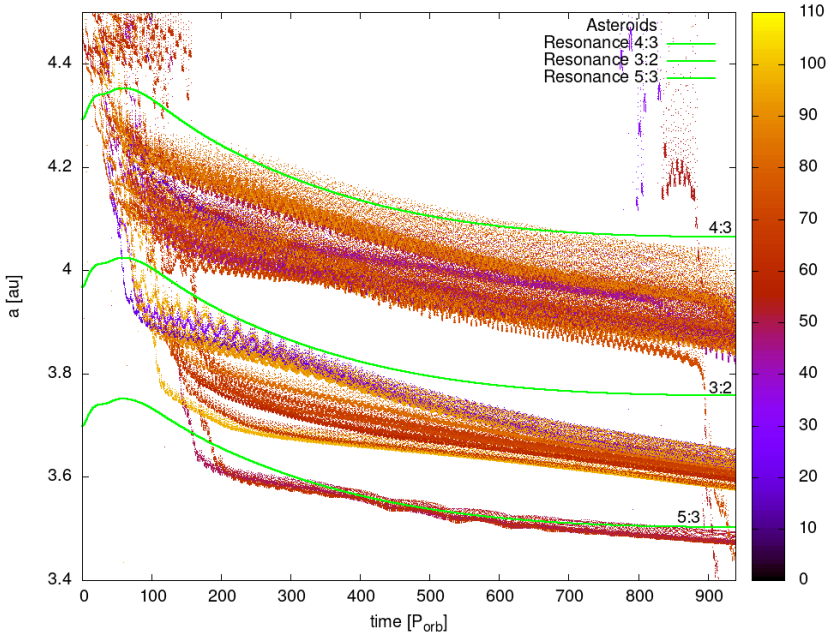

Figure 3.7: Temporal evolution of the semi-major axis of scattered planetesimals. This figure is zoomed in version of Figure 3.2. Highlighted in green are mean-motion resonances 4:3, 3:2, 5:3 with Jupiter. Platesimals slowly migrate inwards (due to drag), past these resonances.

effect is clearly visible, further scattering the planetesimal inwards, as they jump over them.

The inward migration is very slow and we would need at least another 40 kyr of evolution for planetesimals to reach the next resonances like the 2:1, where they could get captured. Another problem we are facing is the proximity of the inner boundary, which is at 2.8 au.

3.2.5 Analysis of pebble distribution

Looking at the pebble disk, we can see it acts very similarly to the gaseous disk. The proto-Jupiter quickly opens a gap and accretes all the pebbles onto itself, as shown in Figure 3.8. In this figure, we can also see in detail Jupiter's clearing of the gap, leaving an under-density right behind it, which is then filled again by migrating pebbles. Importantly, there is not any substantial concentration of pebbles near the L4/L5 points. Moreover, there are no noticeable pressure maximum barriers on the outside nor the inside of the gap, which would block the pebble flow or slow-down the migration of planetesimals.

3.3 Scenario with eccentric and inclined planetesimals

In the first simulation, the final inclinations of planetesimals were too small compared to the observed inclinations of Trojans, but we can assume that planetesimals were already on highly inclined orbits prior to migrating towards proto-Jupiter's Hill sphere. So in our next simulation, all parameters remain the same (described in Section 3.1), except for the initial inclinations and eccentricities

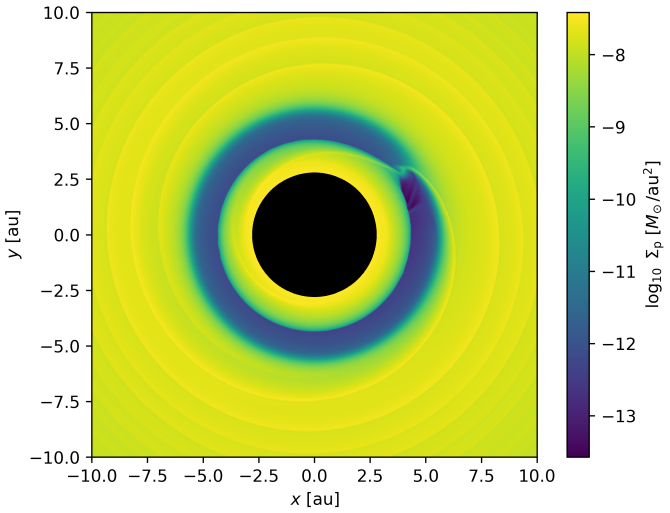

Figure 3.8: The surface density Σ_p of pebbles in the disk after 6 kyr of evolution, when Proto-Jupiter opened a gap. There is a noticeable under-density right behind proto-Jupiter, as recently cleared pebbles did not have a chance to spread again.

of planetesimals. The inclinations were randomly assigned from the interval $[10°, 30°]$ and the eccentricities from $[0, 0.1]$.

The simulation ran for 10 kyr, or 900 Jupiter orbits. The capture efficiency almost doubled to more than 50%. This is caused by the fact that the eccentric orbits allow planetesimals from further out to better interact with proto-Jupiter, thus getting captured.

If a planetesimal with high inclination is captured by the expanding proto-Jupiter, it retains its inclination, thanks to very low gas density and drag in Jupiter's gap. The inclinations of all other planetesimals not captured by the proto-Jupiter decrease to below 5°. The distribution of inclinations of planetesimal at the end of the simulation is in shown in Figure 3.9.

The captured trajectories are similar in nature to trajectories in the first simulation, but are no longer as cold, due to having substantial eccentricities and inclinations as mentioned above. Most of the orbits still began as horseshoes and in time they become tadpole, with a decreasing amplitude of libration, but here we have many outliers, which either stay on horseshoe orbits with very long orbital periods , or enter tadpole orbits temporarily, for multiple kyr, and then get back on the horseshoe. The decrease in amplitudes of libration is generally slower, with some planetesimal seeing no decrease, and for the whole time span of simulation staying on tadpole orbits, spanning almost 150°.

3.4 Scenarios with eccentric and inclined Jupiter

During planetary migration in protoplanetary disks, hydrodynamic phenomena such as the "hot trail" effect, described in Chrenko et al. (2017), Eklund & Masset (2017), can push planetary embryos to eccentric and inclined orbits. To account for these effects, we set our third simulation so that proto-Jupiter has an eccentricity of 0.05 and an inclination of 5. All other initial parameters remain the same as in the first simulation, described in Section 3.1.

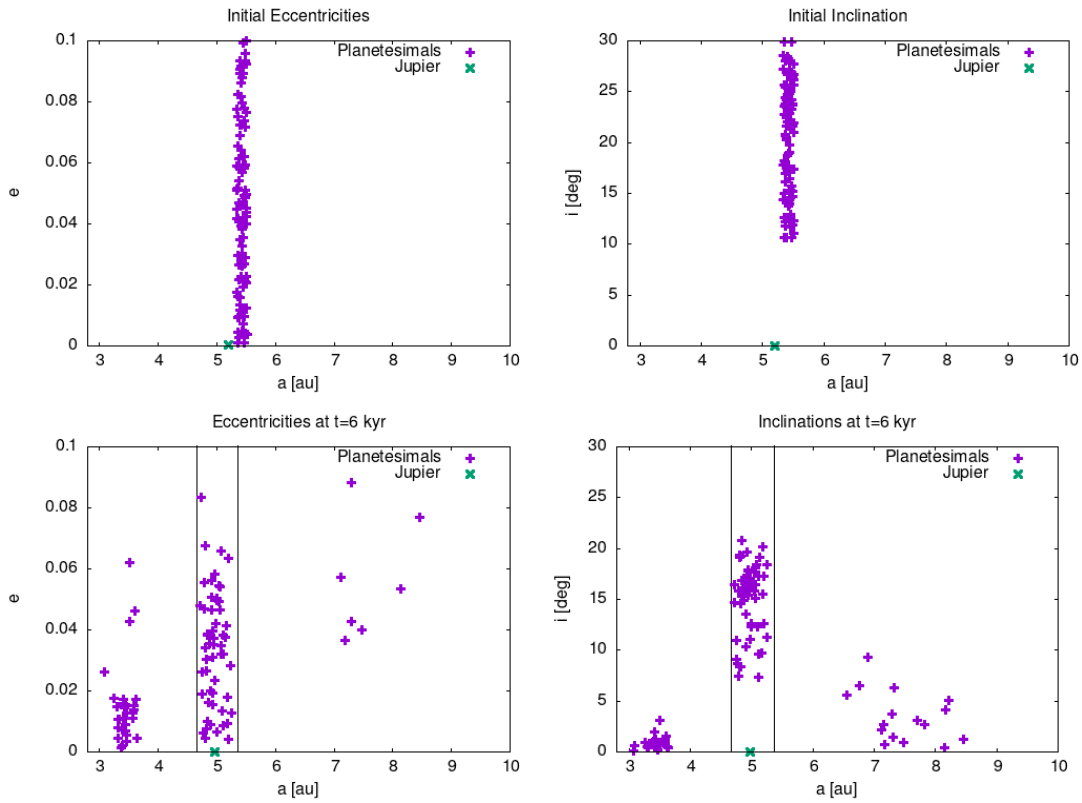

Figure 3.9: Initial and evolved eccentricities and inclinations of proto-Jupiter and 100 planetesimals from the second simulation. The figure is similar to Figure 3.3, except the initial eccentricities and inclinations of planetesimal are non-zero, as shown, in the left plots. The eccentricities and inclinations of captured planetesimals are similar to the initial values, compared to the scattered planetesimals, which were damped by drag. Again, we can compare figure this to Figures 3.10, 3.11, where we modify the initial eccentricities of proto-Jupiter.

3.4.1 Cold planetesimal orbits

First, we simulated a scenario where *only* proto-Jupiter had initial inclination and eccentricity ($e = 0.05$, $i = 5°$), while planetesimals were still on circular planar orbits. The simulation ran for 10 kyr.

During the accretion and opening of the gap, Jupiter's eccentricity and inclination decreased and stabilized close to zero. Nevertheless planetesimals captured by proto-Jupiter were exited to eccentricities up to 0.05 and the inclination up to $i = 5°$, as shown in Figure 3.10.

The capture efficiency substantially decreased in this model, down to 4 captured planetesimals out of the 100. In contrast to our previous model, the capture is not stable. After the initial 50 orbits, the number of captured planetesimal is similar to the first simulation (30), but as the evolution continues, the eccentric Jupiter loses more than 80% of them.

The captured planetesimals mostly stay on horseshoe orbits, which libration amplitude allows for close encounters with proto-Jupiter, ending about 10° from it. Compared to the previous, stable simulations, this is 5° to −10° less. This eventually causes another close encounter with proto-Jupiter and an ejection of the planetesimal.

The planetesimals that transition to tadpole orbits do not decrease their libration amplitude like in our first simulation. Conversely, after a few thousand years their unstable orbits leave the tadpole region and return to the horseshoe; this is commonly caused by another close interaction with proto-Jupiter and is usually followed by leaving the proto-Jupiter orbit entirely.

The eccentric Jupiter also migrates inwards faster, in the span of 10 kyr, migrating from 5.2 au to around 4.85 au, which is 0.1 more than without eccentricity.

3.4.2 Inclined planetesimal orbits

Next, we simulated a scenario, where *both* proto-Jupiter and planetesimals have non-zero initial eccentricities and inclinations. The initial orbital elements of planetesimals are the same as in the second simulation.

Similarly as in the third simulation, Jupiter's eccentricity and inclination are damped close to zero. Even though the initial eccentricities and inclinations are high, the capture efficiency is still around 40%, moreover the orbits of captured planetesimals are stable, because the close encounters with proto-Jupiter are rare.

When planetesimals are initially on eccentric orbits, the eccentric proto-Jupiter has little or no effect on them, and the eccentricity evolves similarly as in the case with eccentric planetesimals. Inclinations also evolve similarly to our second simulation. (Figure 3.11)

The transition from horseshoe to tadpole orbits is less common, and planetesimals are mostly staying on horseshoe orbits.

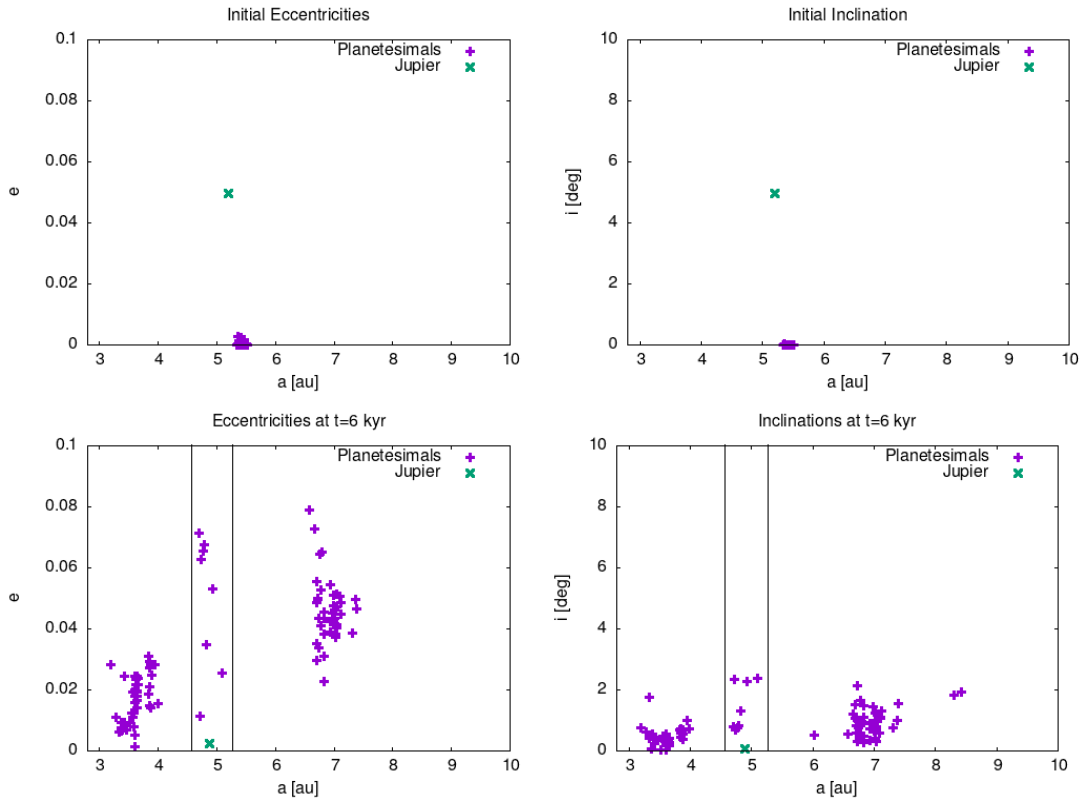

Figure 3.10: Initial and evolved eccentricities and inclinations of proto-Jupiter and 100 plantesimals from the third simulation. The figure is similar to Figure 3.3, except here, the initial eccentricities and inclinations of proto-Jupiter are non-zero, as shown in left plots. The high initial e and i of proto-Jupiter are damped during its growth. However the eccentricities of captured planetesimals are brought up in the course of the simulation to proto-Jupiter's initial eccentricity. The inclinations of captured planetesimals stay low (bellow 2.5°) during the whole simulation. These is a notable decrease in capture efficiency.

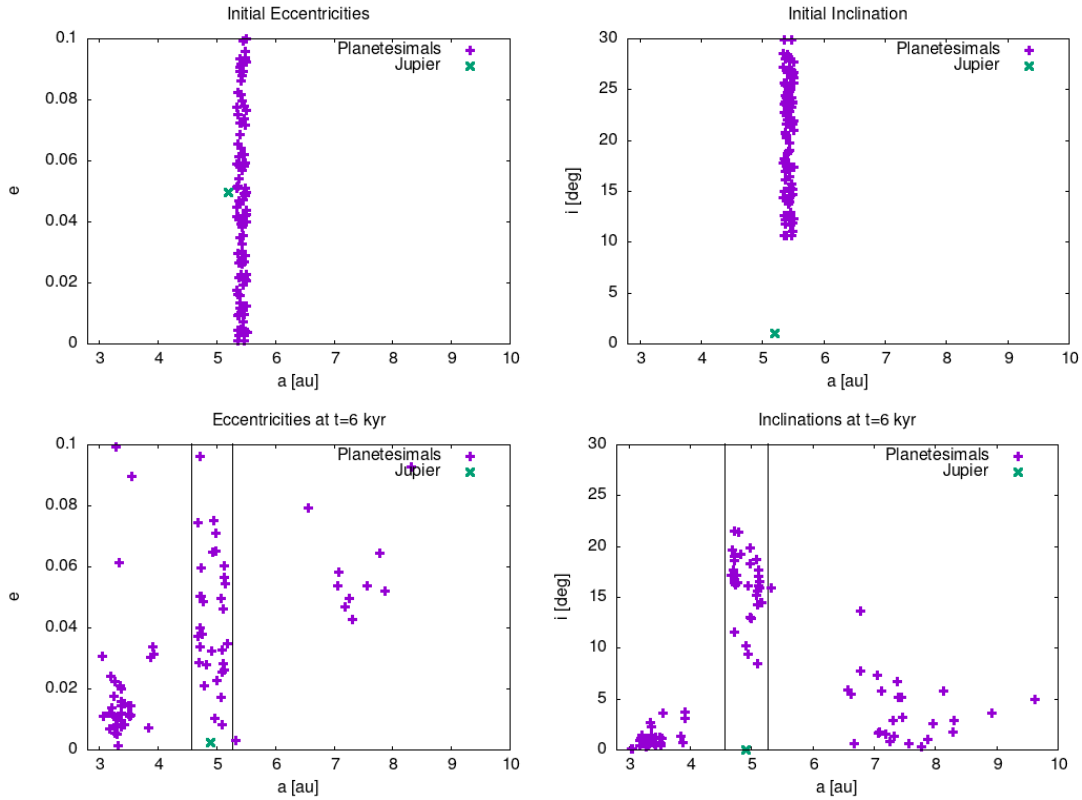

Figure 3.11: Initial and evolved eccentricities and inclinations of proto-Jupiter and 100 planetesimals from the fourth simulation. The figure is similar to Figure 3.3, except here, the initial eccentricities and inclinations of both proto-Jupiter and planetesimals are non-zero, as shown in left plots. The initial eccentricity and inclination of proto-Jupiter are dampened like in Figure 3.10, and the eccentricities and inclination of planetesimals evolve similarly as in Figure 3.9.

4. Models for different planetesimal sizes

In this chapter, we investigate, how the size of planetesimals affects their orbital evolution, in the vicinity of growing Jupiter, and their potential capture. The most notable difference, in the forces acting on these bigger vs smaller bodies, is the aerodynamic drag force.

4.1 Models for 10 km asteroids

We start with a series of simulations using planetesimals with diameters $d = 10\,\mathrm{km}$. The drag force acting on these bodies is relatively low. Using the method described in Section 3.2.1, we calculated the drag acting on a planetesimal on a circular orbit at 5.2 au as $a_{\mathrm{drag}} = 1 \times 10^{-13}\,\mathrm{m\,s^{-2}}$. This is three orders of magnitude lower than for 100 m bodies. The gravity is at this distance $a_{\mathrm{grav}} = 2.08 \times 10^{-4}\,\mathrm{m\,s^{-2}}$, which means we would need at least 63 years for drag to have an effect similar to one-second gravitational effect.

In this scenario, we use the same initial conditions as in the third simulation, described in Section 3.4.1. This means we assum a $20M_{\mathrm{E}}$ proto-Jupiter set up on an eccentric inclined orbit ($e = 0.5$, $i = 5°$). The orbits of planetesimals are circular, with zero eccentricities and inclinations. The only difference here is that the planetesimals are 10 km in diameter.

The evolution 14 kyr is shown in Figure 4.1. During this time proto-Jupiter grew from $20M_{\mathrm{E}}$ to over $320M_{\mathrm{E}}$ and interacted with planetesimals placed near its Hill sphere. The initial eccentricity and inclination of Jupiter are again damped close to zero during the first 3.5 kyr. The first Jupiter planetesimal interaction is the same as described in Section 3.2.2. After the first interaction 27 out of the 100 planetesimals were captured on horseshoe orbits around Jupiter. The rest was scattered inwards or outwards on very high eccentricities up to 0.6 and inclinations up to 8°. The eccentricities and inclinations at 6 and 12 kyr are shown in Figure 4.2.

Similarly to simulation from Section 3.4.1, the horseshoe orbits of captured planetesimals are very unstable. Moreover, in this scenario, all of the previously captured Trojans had another close interaction with proto-Jupiter and thus were scattered out of its orbit. This result is in accordance with results of Marzari & Scholl (1998), who simulated similar capture of Trojans by growth of a protoplanet, but without the hydrodynamical forces, which are, in this case, indeed negligible.

Due to the low drag force, the planetesimal eccentricities decrease very slowly, while they migrate outwards or inwards. Outward migration and resonances are again not very interesting because our simulation does not contain Saturn and other giant plantes. On the other hand, planetesimals that migrate inwards get captured in the 3:2 and 2:1 mean-motion resonances; the latter one is clearly visible in Figure 4.1.

If we initially place planetesimals on highly eccentric and inclined orbits, they get captured on stable orbits and retain the inclinations after getting captured,

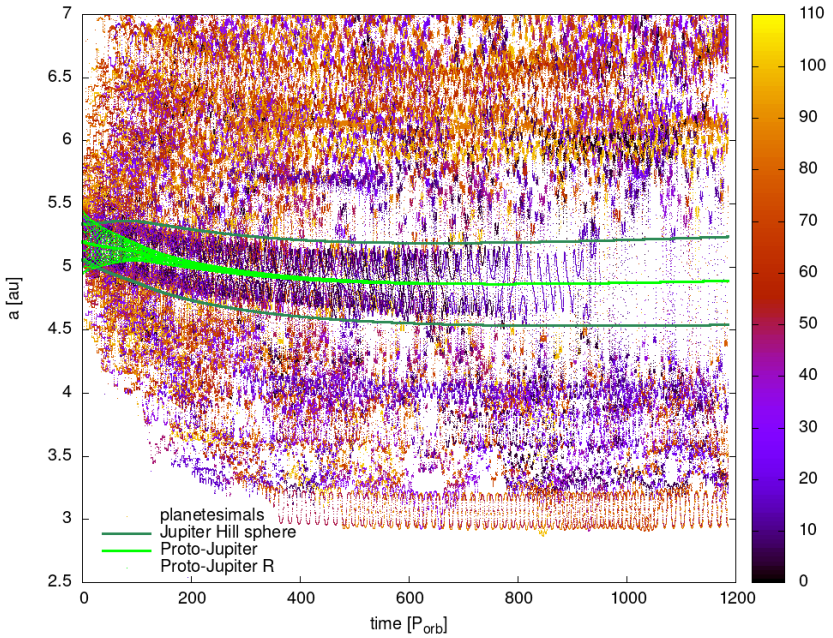

Figure 4.1: Temporal evolution of the semi-major axis of eccentric proto-Jupiter and 10 km planetesimals, similar to Figure 3.2. Captured planetesimals gradually leave the horseshoe orbits until none is left in the vicinity of Jupiter's orbit. The scattered planetesimal migrate outwards and inwards. There is a single notable planetesimal captured in 2:1 mean-motion resonance (just above 3 au).

the same as in Section 3.4.2. The only difference is that here, the drag force outside Jupiter's gap is not strong enough to damp the inclinations of free planetesimals, thus both the free and captured planetesimals have similar inclinations, around their initial values.

4.2 Models for 10 m asteroids

Finally, we simulated a capture of 10-meter-sized planetesimals. The initial conditions are again the same as in the previous simulation. Proto-Jupiter is initialized on an eccentric inclined orbit, and in the first 300 orbits, opens a gap, accretes $300 M_{\mathrm{E}}$ of gas, and damps its eccentricity and inclination to zero. All planetesimals are initially on circular planar orbits.

The drag force acting on planetesimals is strong enough to damp the eccentricities, gained after the first encounter with proto-Jupiter, in a matter of a few orbits. On a circular orbit at 5.2 au, the acceleration from drag is around $a_{\mathrm{drag}} = 1 \times 10^{-9}$ and on an eccentric orbit the acceleration reaches up to $a_{\mathrm{drag}} = 1 \times 10^{-6}$, which is only two orders of magnitude less than the gravitational acceleration.

Because the drag acceleration is so substantial, only the planetesimals that retain any eccentricity or inclination are the ones that got captured by proto-Jupiter and thus are orbiting in the gap, where only little gas was left. For this reason, the orbits of captured planetesimals are stable; there are no cases of escaping planetesimals like in the simulation with 10 km ones. However, final inclinations are too low (1° vs. 30°) compare to observations.

The capture is very reminiscent of the first simulation, capturing, exclusively,

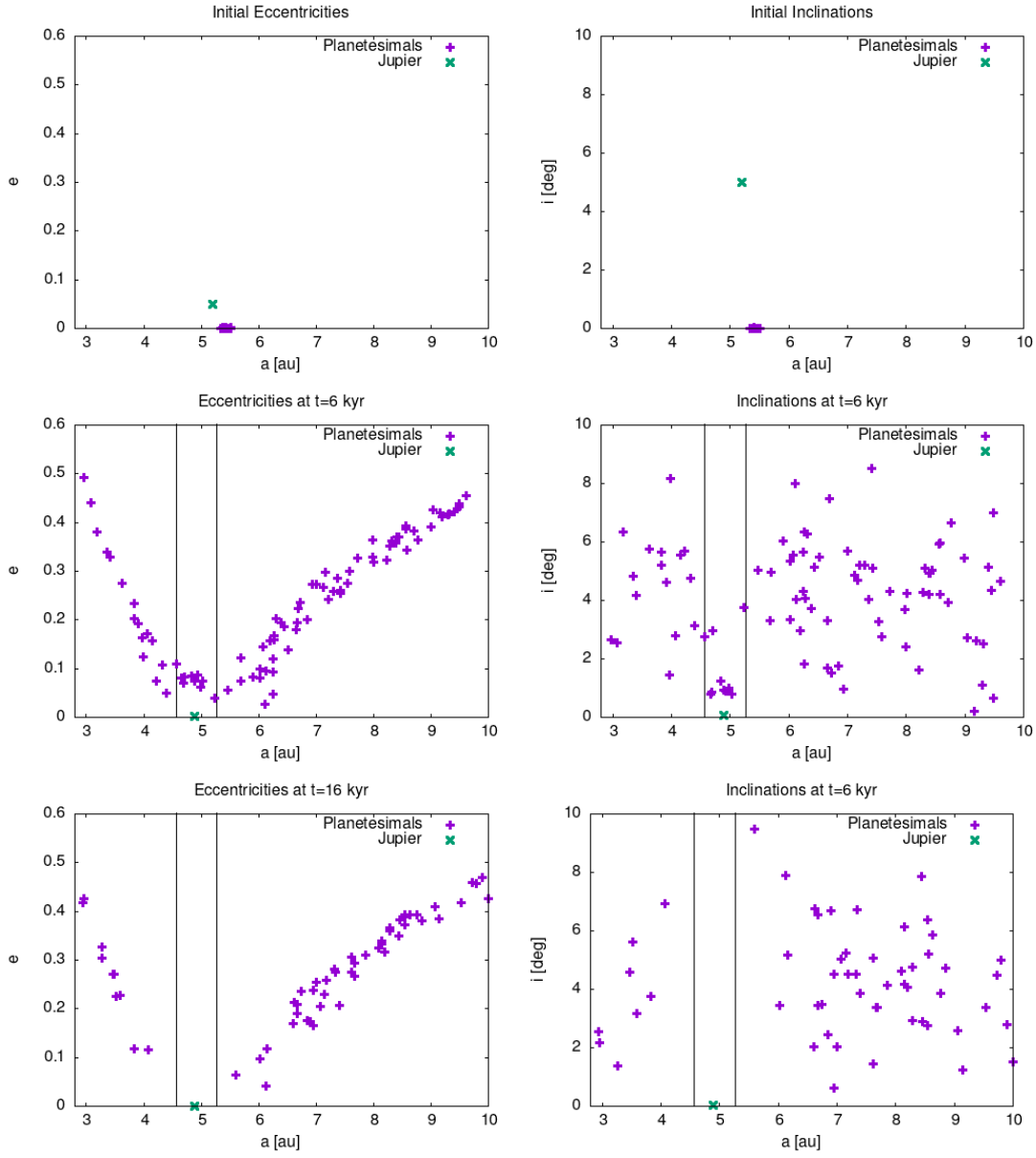

Figure 4.2: The initial and evolved eccentricities and inclinations of proto-Jupiter and 10km planetesimals, similar to Figure 3.10. The planetesimals do not lose eccentricities, due to their size and migrate outwards and inwards. By the end of simulation, no planetesimal remains in Jupiter's orbit.

the nearest 30 planetesimals, with numerous transitions from horseshoe to tadpole orbits, including the subsequent shortening of libration amplitude.

Table 4.1: Summary of our simulations. In our model, the initial conditions for Jupiter on eccentric orbit are $e = 0.05$ and $i = 5°$ and for planetesimals $e = [0, 0.1]$ and $i = [10°, 30°]$. The eccentricity and inclination are the maximal values of captured pletesimals.

No.	Initial conditions	Timespan	Efficiency	e	i
1.	circ. Jup., circ. 100m pl.	11 kyr	29%	0.01	0.01°
2.	circ. Jup., ecc. 100m pl.	10 kyr	52%	0.06	20°
3.	ecc. Jup., circ. 100m pl.	10 kyr	6%	0.08	**2**°
4.	ecc. Jup., ecc 100m pl.	6 kyr	40%	0.1	20°
5.	ecc. Jup., circ. 10km pl.	14 kyr	0%	-	-
6.	ecc. Jup., circ. 10m pl.	10 kyr	25%	0.04	**1.5**°

Conclusions

In this thesis, we studied a capture of planetesimals by rapidly accreting proto-Jupiter. All of our simulations were done using the hydrodynamic Fargo-Thorin code (Chrenko et al. 2017), simulating a two-fluid (gas and pebbles) protoplanetary disk with an embedded planetary embryo. The proto-Jupiter was initially placed close to 5.2 au and its feeding zone is just behind proto-Jupiter's Hill sphere, in the interval $[5.34, 5.51]$ au. Proto-Jupiter rapidly accretes mass and almost immediately opens a gap. We simulated multiple scenarios with differing initial eccentricities and inclinations of proto-Jupiter and 100 m planetesimals and also examined scenarios with 10 km and 10 m planetesimals.

The first scenario, with both $20 M_{\mathrm{E}}$ proto-Jupiter and 100 m planetesimals on circular orbits, is considered a reference scenario. It gave us insight into the mechanics of Trojan capture by growing protoplanets and the evolution of captured orbits, librating in the 1:1 mean-motion resonance with proto-Jupiter. The planetesimals were initially captured on horseshoe orbits, transitioned onto tadpole orbits, and then slowly decreased their libration amplitudes due to aerodynamic drag. It also gave us a reference capture efficiency of about 30%.

The second scenario, with highly inclined (10° to 30°) planetesimal orbits, showed us the dependence on the initial inclination, as the capture of the inclined eccentric planetesimals was more efficient, with efficiency over 50%. The planetesimals mostly retained their high inclinations.

The third and fourth scenarios were simulated with proto-Jupiter initially on eccentric inclined orbit ($e = 0.05$, $i = 5°$), with hopes that Jupiter would through the capturing interaction send the planetesimals onto highly inclined orbits. However, the final Trojan inclinations were only around 2.5°, which is very low compared to observation ($i = 30°$). Moreover, the orbits of these Trojans were not stable; in the course of time the planetesimals interacted with proto-Jupiter again and were ejected out of its orbit. This loss of Trojans and the low inclinations, however, could be solved again by high initial eccentricities and inclinations of planetesimals.

The simulations in Chapter 4 had proto-Jupiter also on the inclined eccentric orbit, but this time the planetesimals were larger (10 km in diameter) or smaller (10 m). The different sizes of planetesimals implied different drag acting on them. For the 10 km bodies, this resulted in even more losses of captured planetesimals to the degree, that no Trojan was left in Jupiter's orbit after 14 kyr of evolution. In the case of 10 m bodies, the very high drag stabilized their orbits, but their captured inclinations were even smaller, $i = 1.5°$.

We conclude that the capture of Trojans by the growth of eccentric Jupiter is unlikely, as it would require the planetesimals to orbit in the disk on highly inclined orbits, prior to interacting with Jupiter or there would have to be an external dynamical excitation during the subsequent evolution of the Solar System.

Future work. Alternative scenarios certainly exist, with different parameter values, that could change the Trojan capture. For example, simulations with a less turbulent, magnetically-inactive disk, with the kinematic viscosity one or more orders of magnitude lower. As a continuation of this work, one could also investigate the dynamics of planetesimal excitation, either before or after capture. One possibility is a temporary capture of a massive planetesimal or embryo and its influence on the remaining planetesimal inclinations.

Bibliography

[1] Balbus, S. A. & Hawley, J. F. (1991), 'A powerful local shear instability in weakly magnetized disks. I. linear analysis', *Astrophys. J.* **376**, 214.

[2] Brož, M., Chrenko, O., Nesvorný, D. & Dauphas, N. (2021), 'Early terrestrial planet formation by torque-driven convergent migration of planetary embryos', *Nature Astronomy* **5**, 898–902.

[3] Brož, M. & Rozehnal, J. (2011), 'Eurybates - the only asteroid family among Trojans?', *Mon. Not. R. Astron. Soc.* **414**(1), 565–574.

[4] Brož, M. (2022), *Hydrodynamika v astronomii*.
URL: *https://sirrah.troja.mff.cuni.cz/~mira/hydrodynamika/*

[5] Chrenko, O., Brož, M. & Lambrechts, M. (2017), 'Eccentricity excitation and merging of planetary embryos heated by pebble accretion', *Astron. Astrophys.* **606**, A114.

[6] Eklund, H. & Masset, F. S. (2017), 'Evolution of eccentricity and inclination of hot protoplanets embedded in radiative discs', *Mon. Not. R. Astron. Soc.* **469**(1), 206–217.

[7] Hayashi, C. (1981), 'Structure of the solar nebula, growth and decay of magnetic fields and effects of magnetic and turbulent viscosities on the nebula', *Progress of Theoretical Physics Supplement* **70**, 35–53.

[8] Lovett, E. O. (1895), 'The great inequality of Jupiter and Saturn', *Astrophys. J.* **15**, 113–127.

[9] Lyra, W., Johansen, A., Klahr, H. & Piskunov, N. (2009), 'Standing on the shoulders of giants. Trojan Earths and vortex trapping in low mass self-gravitating protoplanetary disks of gas and solids', *Astron. Astrophys.* **493**(3), 1125–1139.

[10] Marzari, F. & Scholl, H. (1998), 'The growth of Jupiter and Saturn and the capture of Trojans', *Astron. Astrophys.* **339**, 278–285.

[11] Masset, F. (2000), 'FARGO: A fast eulerian transport algorithm for differentially rotating disks', *Astron. Astrophys.* **141**, 165–173.

[12] *Minor Planet Center* (2023).
URL: *https://www.minorplanetcenter.net/*

[13] Morbidelli, A., Brasser, R., Gomes, R., Levison, H. F. & Tsiganis, K. (2010), 'Evidence from the Asteroid Belt for a violent past evolution of Jupiter's orbit', *Astrophys. J.* **140**(5), 1391–1401.

[14] Morbidelli, A., Levison, H. F., Tsiganis, K. & Gomes, R. (2005), 'Chaotic capture of Jupiter's Trojan asteroids in the early Solar System', *Nature* **435**(7041), 462–465.

[15] Nesvorný, D. (2018), 'Dynamical evolution of the early Solar System', *Annu. Rev. Astron. Astrophys.* **56**, 137–174.

[16] Nesvorný, D., Vokrouhlický, D. & Morbidelli, A. (2013), 'Capture of Trojans by jumping Jupiter', *Astrophys. J.* **768**(1), 45.

[17] Nicholson, S. B. (1961), 'The Trojan Asteroids', *Leaflet of the Astronomical Society of the Pacific* **8**(381), 239.

[18] Pirani, S., Johansen, A., Bitsch, B., Mustill, A. J. & Turrini, D. (2019), 'Consequences of planetary migration on the minor bodies of the early solar system', *Astron. Astrophys.* **623**, A169.

[19] Pollack, J. B., Hubickyj, O., Bodenheimer, P., Lissauer, J. J., Podolak, M. & Greenzweig, Y. (1996), 'Formation of the giant planets by concurrent accretion of solids and gas', *Icarus* **124**(1), 62–85.

[20] Rozehnal, J., Brož, M., Nesvorný, D., Durda, D. D., Walsh, K., Richardson, D. C. & Asphaug, E. (2016), 'Hektor - an exceptional D-type family among Jovian Trojans', *Mon. Not. R. Astron. Soc.* **462**(3), 2319–2332.

[21] Shakura, N. I. & Sunyaev, R. A. (1973), 'Black holes in binary systems. Observational appearance.', *Astron. Astrophys.* **24**, 337–355.

[22] Szabó, G. M., Ivezić, Ž., Jurić, M. & Lupton, R. (2007), 'The properties of Jovian Trojan asteroids listed in SDSS Moving Object Catalogue 3', *Mon. Not. R. Astron. Soc.* **377**(4), 1393–1406.

[23] Tsiganis, K., Gomes, R., Morbidelli, A. & Levison, H. F. (2005), 'Origin of the orbital architecture of the giant planets of the Solar System', *Nature* **435**(7041), 459–461.

[24] Vinogradova, T. A. (2020), Families among the Hildas and Trojans, *in* 'IAU General Assembly', pp. 24–25.

[25] Vinogradova, T. A. & Chernetenko, Y. A. (2015), 'Total mass of the Jupiter Trojans', *Solar System Research* **49**(6), 391–397.

[26] Wolf, M. (1892), 'Photographische Aufnahmen von kleinen Planeten', *Astronomische Nachrichten* **129**(22), 337.

[27] Wolf, M. (1906), 'Photographische Aufnahmen von kleinen Planeten', *Astronomische Nachrichten* **172**, 387.

[28] Wolf, M. (1907), 'Photographische Aufnahmen von kleinen Planeten', *Astronomische Nachrichten* **174**(4), 63.

[29] Zhu, Z., Hartmann, L., Nelson, R. P. & Gammie, C. F. (2012), 'Challenges in forming planets by gravitational instability: disk irradiation and clump migration, accretion, and tidal destruction', *Astrophys. J.* **746**(1), 110.